Contents lists available at ScienceDirect

Arabian Journal of Chemistry

journal homepage: www.ksu.edu.sa

Original article

Na-CDs as an eco-friendly and efficient corrosion inhibitor for Q235 in 1 M HCl

Liming Dong [a], Jingbao Wang [b], Yuyue Ma [a], Yilei Ruan [a], Zhiyong Hu [a], Xuemei Ma [a,*]

[a] School of Chemistry and Chemical Engineering, North University of China, Taiyuan 030051, China
[b] School of Materials Science and Engineering, Beijing University of Chemical Technology, Beijing 100029, China

ARTICLE INFO

Keywords:
Carbon dots
Corrosion inhibitor
Electrochemical test
Adsorption study

ABSTRACT

In this study, a novel type of green and highly efficient Na-CDs corrosion inhibitor was successfully prepared using a hydrothermal method, and its properties were thoroughly characterized. The results revealed that the Na-CDs possessed a uniform nanoscale size distribution and a well-defined graphene lattice structure. The corrosion inhibition performance of Na-CDs at varying concentrations was assessed, and it was found that the corrosion inhibition efficiency initially increased with the increase of concentration, peaking at over 96 % when the concentration reached 150 mg/L, before subsequently declining. Analysis of the adsorption behavior of Na-CDs on the metal surface confirmed that the adsorption process followed the R-P adsorption isotherm, indicative of an almost ideal homogeneous monolayer adsorption. The corrosion inhibition mechanism is the result of forming a protective film on the metal surface by physical adsorption and chemical adsorption, with the bridging role of Cl^- further reinforcing the structure of this film. However, at excessively high concentrations of Na-CDs, desorption occurred, compromising the integrity of the protective film. This study enriches the field of metal-doped carbon dots as corrosion inhibitors and provides insights into the synthesis of carbon dots and the development of carbon dot-based corrosion inhibitors.

1. Introduction

In industrial production, a 1 M HCl solution is often used to scour off scale and rust from carbon steel surface during the pickling process of equipment (Hu et al., 2016; Ye et al., 2020). However, under acidic conditions, carbon steel is vulnerable to corrosive ions, which can lead to severe corrosion, posing significant risks to life and property safety (Gutiérrez et al., 2016). One of the most convenient and effective methods to address this issue is the addition of corrosion inhibitors to the pickling solution (K. Zhang, 2018). Corrosion inhibitors that typically exhibit excellent performance often contain elements such as sulfur, nitrogen, phosphorus, and aromatic rings. These substances are considered adsorption centers, capable of forming coordination with vacant metal surface orbitals, thereby generating a dense protective film that safeguards the metal from corrosion (Abd El-Lateef et al., 2016; Hejazi et al., 2015; Ramezanzadeh et al., 2019). Nevertheless, with the increasingly serious environmental problems, the importance of green development has become increasingly prominent. Traditional corrosion inhibitors are no longer suitable because of their toxicity and environmental pollution. It is imperative to develop environment-friendly and efficient corrosion inhibitors (El-Etre et al., 2005; Y. Zhang et al., 2015).

Carbon dots (CDs), with their exceptional water solubility, excellent, tunable photoluminescence, and straightforward synthesis methods, have attracted widespread attention across various industries since their inception (Abdelhameed et al., 2021; Ai et al., 2023; Almomani et al., 2021; Cao & Guo, 2024; García de Arquer et al., 2021; Miao et al., 2018). The field of metal corrosion prevention is no exception. In 2017, CDs were first used as corrosion inhibitors for carbon steel in 1 M HCl solution (M. Cui et al., 2017), and since then, there has been an increasing amount of reports about CDs as corrosion inhibitors. For instance, Yang et al. (D. Yang et al., 2019) synthesized functionalized CDs using ionic liquids and citric acid, demonstrating corrosion inhibition efficiencies of 91.1 % and 85.7 % for Q235 steel in 1 M HCl and 3.5 wt% NaCl solutions, respectively. Ye et al. (Z. Liu et al., 2020) prepared three series of N-doped CDs (N-CDs) from ammonium citrate, achieving inhibition rates greater than 90 % for Q235 steel in 1 M HCl. Saraswat et al. (Saraswat & Yadav, 2021) produced N,S-doped CDs (N,S-CDs) from citric acid, isoniazid, and thiourea, showing that N,S-CDs provide excellent protection for Q235 carbon steel in HCl solution. Ren et al. (S. Ren et al., 2022) prepared N-CDs and N,S-CDs using salicylic acid, urea,

* Corresponding author.
E-mail address: maxuemei@nuc.edu.cn (X. Ma).

https://doi.org/10.1016/j.arabjc.2024.105660
Received 3 January 2024; Accepted 28 January 2024
Available online 2 February 2024

and thiourea, exploring the protective property of N and N,S co-doped carbon dots on Q235 steel in acidic solution and suggesting that N,S-CDs offer more adsorption anchor points and superior corrosion inhibition than N-CDs. Luo et al. (Luo et al., 2021a) created N,S-CDs using ammonium citrate and methionine by controlling their ratio, examining the impact of sulfur content in N,S-CDs on the corrosion inhibition of Q235 carbon steel in 1 M HCl, and found the best inhibition effect at 10 % sulfur content. These studies indicate that CDs inhibit metal corrosion by forming a protective film through both physical and chemical adsorption on the metal surface. However, research on CDs as corrosion inhibitors has been largely confined to such non-metal-doped carbon dots, significantly limiting the development of CD-based corrosion inhibitors.

Compared to non-metal atoms, metal-ion-doped CDs (M−CDs) can cause significant alterations in optical, electronic, and magnetic properties by changing the electron density distribution and bandgap of CDs (X. Li et al., 2022). This has led to considerable interest in M−CDs for applications in optical sensors, photocatalysis, and electrocatalysis (Guo et al., 2020; Han et al., 2018; Mu et al., 2019; Tian et al., 2018). However, there is scant research on M−CDs as corrosion inhibitors, with only a few studies exploring carbon dots doped with both low-activity metals and non-metal atoms (Padhan et al., 2022; Zeng et al., 2022). There is less research on the corrosion inhibition of metal-ion-doped CDs. The incorporation of metal ions into CDs provides abundant binding sites, modifies the defect states of CDs, and promotes electron transfer, enabling M−CDs to bind more effectively to the metal surface. In addition, the metal ions in M−CDs can react with the corrosive medium and form passive film, thereby avoiding further corrosion of the carbon steel. Given that sodium (Na) is abundant and inexpensive, and its reactivity is far greater than that of iron (Fe), using Na as a doping source to produce Na-doped CDs (Na-CDs) could potentially form a passive film lon the surface of Fe. After adsorption, the excellent reactivity of Na^+ may facilitate generation of protective passive film on the metal surface, and Na^+ can also combine with Cl^- to form NaCl, which is good water-solubility and flows easily with water after pickling, without affecting the condition of the equipment or piping. Furthermore, the corrosion inhibition mechanism of Na-CDs might differ from that of non-metal atom-doped CDs, making the development and performance study of Na-CDs as corrosion inhibitors of great necessity.

In this study, Na-CDs were synthesized using a hydrothermal method. The structure and morphology of Na-CDs were comprehensively analyzed using Fourier-transform infrared spectroscopy (FTIR), Raman spectroscopy, X-ray photoelectron spectroscopy (XPS), X-ray diffraction (XRD), and transmission electron microscopy (TEM). The corrosion inhibition effect of Na-CDs on carbon steel in 1 M HCl solution was assessed through weight loss experiments and electrochemical tests. Scanning electron microscopy (SEM) and energy-dispersive X-ray spectroscopy (EDS) were used to examine the surface morphology and elemental distribution of carbon steel under different conditions. The corrosion inhibition mechanism of Na-CDs was analyzed comprehensively.

2. Experimental section

2.1. Materials

Sodium citrate and copper chloride were of analytical grade, purchased from Macklin. Q235 carbon steel samples (0.80 wt% Mn, 0.50 wt % C, 0.37 wt% Si, 0.25 wt% Cu, 0.25 wt% Cr, 0.25 wt% Ni, 0.045 wt% S, 0.04 wt% P and balance Fe) were acquired from Shandong Shengxin Science and Technology Co., Ltd. The specifications of the Q235 samples used for electrochemical tests were 1 cm^3, the electrodes were encapsulated using an epoxy resin and exposed to a surface of 1 cm^2 due to electrochemical testing. The Q235 samples used for weight loss experiments were initially 3.55 cm × 2.8 cm × 0.4 cm in size, with a diameter of 0.4 cm. All Q235 carbon steels are polished with 200 to 2,000 pieces of silicon carbide paper before testing, and samples are cleaned using ultrasonic waves using industrial ethanol. Concentrated hydrochloric acid solution purchased from Tianjin Damao Chemical Reagent Factory. Deionized water was produced in-house in the laboratory.

2.2. Preparation of Sodium-Doped carbon dots (Na-CDs)

Na-CDs were prepared using a hydrothermal method, as shown in Fig. 1, resembled Ren et al. (X. Ren et al., 2015) in method. Initially, 0.1 M sodium citrate and 0.1 M copper chloride were dissolved in 100 mL of deionized water. The resulting solution was transferred to a 200 mL polytetrafluoroethylene (PTFE)-lined autoclave. The autoclave was maintained at 200 °C for 5 h. After the solution cooled naturally to room temperature, a 0.22 μm aqueous system filter membrane was used to filter out insoluble large particles from the resultant brown solution. The filtered solution was then placed into a 1000 kDa dialysis bag and dialyzed in deionized water for 24 h, with the water changed every 6 h. The dialyzed solution was lyophilized to obtain a yellow–brown solid product, which is the Na-CDs.

2.3. Characterization of Na-CDs

The structural morphology, size distribution, and crystalline characteristics of the synthesized Na-CDs were investigated using XRD on a Panalytical Empyrean system (Netherlands) and TEM on a FEI Talos F200X G2 instrument (USA). Raman spectroscopy, employing a Horiba LabRAM HR Evolution (Japan) with a laser excitation wavelength of 532 nm, was utilized to assess the graphitization level of Na-CDs across a spectral range of 800–2200 cm^{-1}. FTIR analyses were performed on a Thermo Fisher Nicolet iS50 (USA) within the range of 600–4000 cm^{-1}, to elucidate the functional groups present in Na-CDs. The electronic structure and elemental composition were further elucidated by XPS on a Thermo Scientific K-Alpha system (USA). The colloidal stability of Na-CDs in a 1 M HCl solution was characterized by measuring their zeta potential using a zeta potential analyzer (Brookhaven, USA).

2.4. Weight loss measurements

The dimensions of the Q235 carbon steel samples for the weight loss experiments are detailed in Table S1. Samples were immersed in 1 M HCl solution both in the absence and presence of varying concentrations of Na-CDs for a duration of 24 h, after soaking, the Q235 sample was slowly washed with a small flow of deionized water. The mass of the samples was recorded with a precision of 0.1 mg before and after immersion, and the measurements were repeated thrice to obtain an average value. The experiments were conducted in a 100 mL double-walled beaker to maintain a constant temperature of 289 K throughout the process.

2.5. Electrochemical measurements

Electrochemical assays were designed as follows: Na-CDs were dissolved in 1 M HCl solution to prepare inhibited solutions with concentrations of 50, 100, 150, and 200 mg/L, respectively. ACS2350M electrochemical workstation (CORRTEST, China) was utilized to perform the measurements using a three-electrode system. This system consisted of a saturated calomel electrode (reference electrode), a 1.0 cm^2 platinum sheet (counter electrode), and a Q235 carbon steel working electrode with a 1.0 cm^2 area exposed, the latter being encapsulated in epoxy resin (Jin et al., 2022; J. Wang et al., 2021). Prior to electrochemical impedance spectroscopy (EIS) and potentiodynamic polarization (PDP) tests, a stable open circuit potential was established. Before electrochemical tests, a stable open circuit potential (E_{OCP}) was obtained. The amplitude of sinusoidal potential was 10 mV, and the measurement frequency of electrochemical impedance spectroscopy (EIS) was 10^5Hz ~ 10^{-2}Hz, and the resulting data were processed using

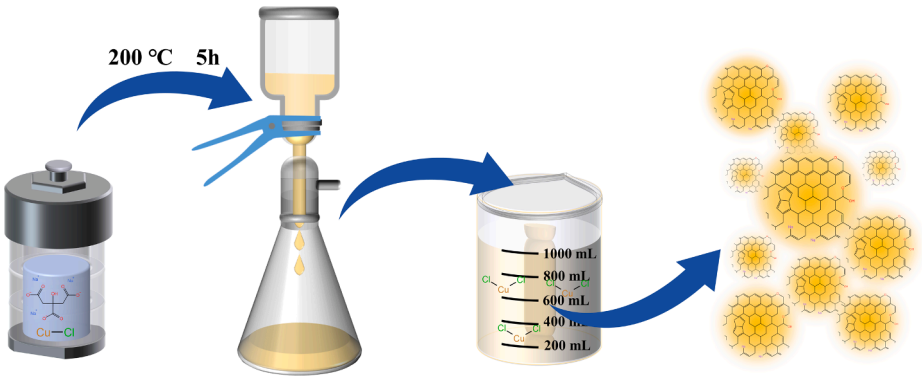

Fig. 1. Schematic diagram of Na-CDs preparation process.

ZSimpWin software. The polarization curves were carried out with E_{OCP} ± 250 mV, and the scanning rate was 0.5 mV/s, and the results were analyzed with CView2 software (Cen et al., 2019b). All electrochemical experiments were performed in triplicate to ensure the reliability of the data.

2.6. Surface characterization

Post weight loss testing, the Q235 carbon steel samples were retrieved, rinsed with deionized water, and subsequently dried using a stream of cold, dry air. Surface morphology of the carbon steel, was examined using a Scanning Electron Microscope (TESCAN MIRA LMS, Czech Republic). Energy-dispersive X-ray spectroscopy (EDS) was employed to analyze the elemental composition of the metal surfaces under various conditions.

3. Results and discussion

3.1. Structural characterization of Na-CDs

TEM and HRTEM results are shown in Fig. 2a and 2b, respectively. A size distribution of 100 randomly selected Na-CDs, as shown in the inset of Fig. 2a, indicates that the sizes are primarily concentrated between 2 and 5 nm, with an average size of 3.62 nm. As shown in Fig. 2b, the lattice stripes of Na-CDs are very clear, the illustration shown is a high resolution image of the selected carbon points, showing the (1 0 2) and (1 0 0) crystal faces of Na-CDs with a spacing of 0.25 and 0.21 nm, respectively (Cen et al., 2019a; Dang et al., 2018; L. Wang et al., 2014). Raman spectrum test was performed at 532 nm laser wavelength, as shown in Fig. 2d. The two peaks at 1355.48 and 1591.71 cm^{-1} are the D and G bands of Na-CDs, respectively. These bands are associated with the vibrations of sp^3 and sp^2 hybridized carbon within the hexagonal

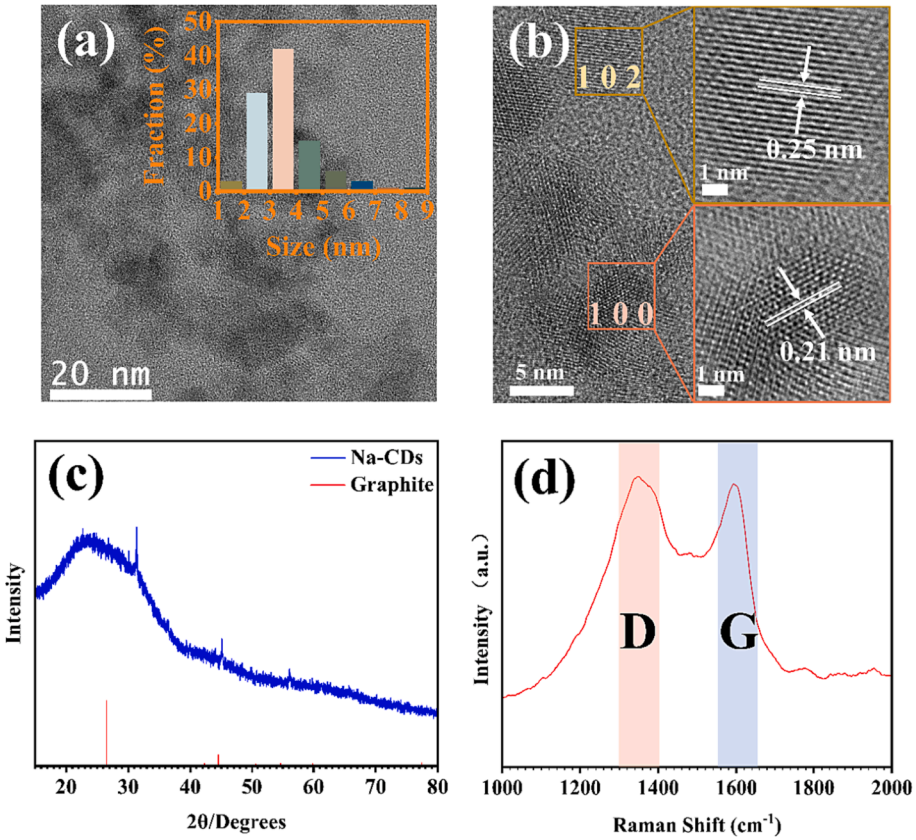

Fig. 2. (a) TEM images and particle size distribution of Na-CDs, (b)HRTEM images, (c) and (d) are XRD and RAMAN data images of Na-CDs, respectively.

lattice of graphite. The intensity ratio of the D to G bands (ID/IG) is 1.02, reflecting the degree of graphitization of Na-CDs (Q. Yang et al., 2018).

The infrared spectroscopy data are presented in Fig. 3. The peaks at 3423, 2962, 1571, 1394 and 1072 cm^{-1} can be attributed to the vibrations of O–H, C–H, C = C, C–H and C-O-C, respectively (W. Li et al., 2019; Rashid et al., 2012).

The elemental composition and corresponding valence states of Na-CDs were obtained by XPS. The full spectrum of XPS measurement is shown in Fig. 4a, and it can be seen that only C, O, and Na elements are contained. The three elements were then analyzed at high resolution. The high-resolution map of C1s is shown in Fig. 4b, where 284.8, 286.5 and 288.3 eV are the characteristic peaks of C–C, O-C = O and C-O-C, respectively (Zhu et al., 2022). Fig. 4c presents the high-resolution O1s spectrum, where peaks at 531.2 eV for C-O, 533.1 eV for C = O, and a feature at 535.5 eV resulting from the sodium Auger peak (Na KLL) were identified through deconvolution (S. Ren et al., 2022). The characteristic peak at 1071.1 eV (Fig. 4d) is attributed to Na 1 s (X. Liu et al., 2022). The results of TEM, XRD, FTIR and XPS show that the prepared Na-CDs have relatively uniform particle size distribution and are rich in functional groups. Because of its rich functional groups and the larger atomic diameter of sodium atoms, the crystal face spacing of Na-CDs is larger than that of graphene. However, no matter what kind of characterization method, the successful preparation of sodium ion doped carbon dots has been proved.

3.2. Weight loss measurements

Weight loss measurement is one of the common methods to evaluate the performance of corrosion inhibitors. By controlling the temperature and time of corrosion reaction and measuring the mass loss of metal samples in corrosive media containing different concentrations of corrosion inhibitors, the performance of inhibitors was analyzed. Corrosion rate (V) and corrosion inhibition efficiency (IE_w%) can be calculated by formulas (Eq. (1)) and (Eq. (2)) (Cen et al., 2019b):

$$V = \frac{W_0 - W}{At} \tag{1}$$

$$IE_w = \frac{V_0 - V}{V_0} \times 100\% \tag{2}$$

In formula (1) and (2), W_0 and W are the weight of Q235 carbon steel before and after weight loss test, respectively. A and t are the surface area and soaking time of the sample, respectively. V_0 and V are the corrosion rates of samples in 1 M HCl solution without and with different concentrations of Na-CDs, respectively. Fig. 5 shows the corrosion inhibition rate of Q235 carbon steel in 1 M HCl solution without and with different concentrations of Na-CDs and the corrosion rate of Q235 carbon steel. The average values of mass loss (ΔW), corrosion rate (V) and corrosion inhibition efficiency (IE_W) of carbon steel at different Na-CDs concentrations are shown in Table 1. All the data of weight loss test are shown in Table S1.

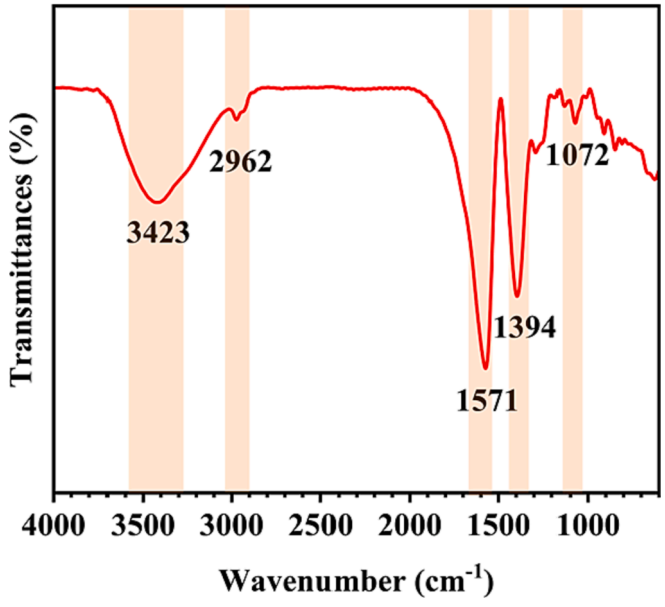

Fig. 3. FTIR spectra.

Compared with the corrosion rate of Q235 carbon steel in 1 M HCl solution without Na-CDs, the addition of Na-CDs significantly reduces the corrosion rate. With the increase of the concentration of Na-CDs, the corrosion rate first increased and then decreased. When the concentration of Na-CDs was 150 mg/L (as show Table S1), the corrosion inhibition efficiency was the highest, reaching 96.07 %, and the corrosion rate was reduced from 0.1635 $g{\cdot}cm^{-2}{\cdot}h^{-1}$ to 0.0064 $g{\cdot}cm^{-2}{\cdot}h^{-1}$, 25.55 times decrease. It is worth noting that even at 50 mg/L, the inhibition efficiency of Na-CDs is about 90 %. However, unlike common CDs corrosion inhibitors, the corrosion inhibition rate increases with the increase of concentration, and when the concentration exceeds 150 mg/L, the inhibition efficiency decreases when reaching 200 mg/L. This may be due to increased interactions between Na-CDs at higher concentrations, or it may be due to increased desorption rates of Na-CDs from metal surfaces at higher concentrations. But overall, the results of the weight loss measurements clearly show that Na-CDs provides excellent protection against carbon steel in 1 M HCl solutions.

3.3. Potentiodynamic polarization (PDP) analysis

Fig. 6(a) displayed the potentiodynamic polarization data for Q235 carbon steel in 1 M HCl solutions without and with various concentrations of Na-CDs at 298 K. It was clearly observed that the addition of Na-CDs to 1 M HCl resulted in a noticeable negative shift in the corrosion potential compared to the blank solution, with the maximum shift being 56.95 mV, which is less than 85 mV. This indicated that Na-CDs acted as a mixed-type corrosion inhibitor (Qiang et al., 2017; Zhao et al., 2022). The cathodic branches of all PDP curves showed a parallel trend, suggesting that the mechanism of the cathodic reaction remained unchanged upon the addition of Na-CDs, while the significant reduction in corrosion current density demonstrated that Na-CDs effectively suppressed the cathodic reaction (Xu et al., 2023). Moreover, the addition of Na-CDs resulted in a distinct plateau region around −0.33 V on the anodic branches, this is due to the adsorption of Na-CDs in the anode region, forming an adsorption film, thus inhibiting the anode reaction, there is an obvious anode passivation zone. When the polarization potential exceeded this value, the current density increased sharply, a phenomenon typically referred to as the desorption potential (E_{des}) (Desimone et al., 2011), where the Na-CDs rapidly desorbed from the metal surface, causing the anodic curve to coincide or nearly coincide with that of the blank condition (Cen et al., 2019a).

The corrosion potential (E_{corr}), corrosion current density (i_{corr}), and the Tafel slopes for the anode and cathode (b_a and b_c) were obtained by fitting the data in the Tafel region near the corrosion potential using CView2 software, as shown in Table 2. The inhibition efficiency IE_{PDP} was calculated using Equation (3) (R. Cui et al., 2011).

$$IE_{PDP} = \frac{i_{corr}^0 - i_{corr}}{i_{corr}} \times 100\% \tag{3}$$

In the formula, where i_{corr}^0 and i_{corr} are the corrosion rates without and with inhibitor, respectively.

It is noteworthy that, unlike many carbon dot inhibitors, the inhibition efficiency of Na-CDs does not increase monotonically with the concentration, and reaches the maximum when the concentration is 150 mg/L. At this concentration, the plateau region was widest and the E_{des} highest, indicating that at this point, the protective film formed by Na-

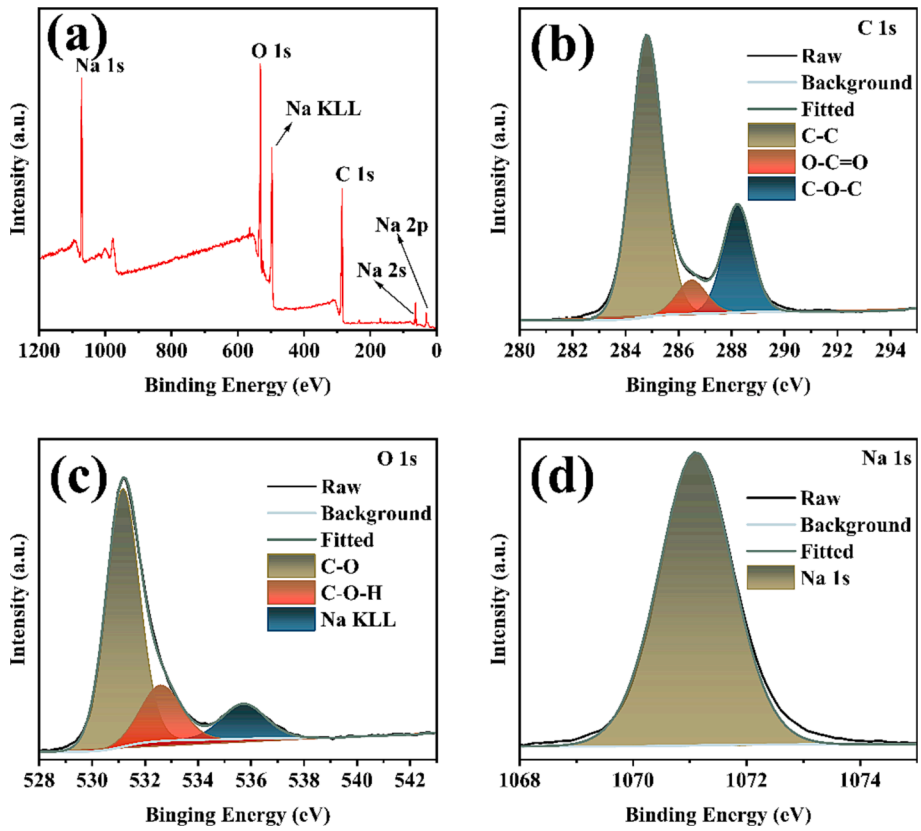

Fig. 4. (a) XPS full spectrum of Na-CDs, and (b)-(d) high-resolution XPS images of C1s, O1s and Na1s, respectively.

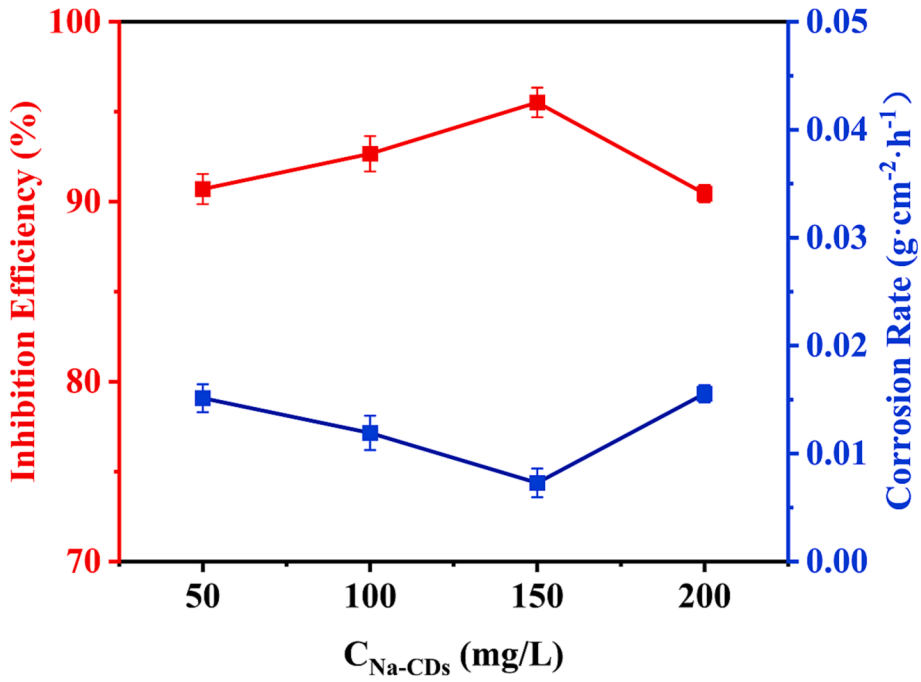

Fig. 5. Corrosion inhibition rate (red) and corrosion rate (blue) of Q235 Carbon steel in 1 M HCl solution containing different concentrations of Na-CDs at 289 K. (For interpretation of the references to colour in this figure legend, the reader is referred to the web version of this article.)

CDs on the metal surface had the strongest adhesion (X. Zhang et al., 2001). When the concentration of Na-CDs exceeds 150 mg/L, the corrosion current will increase sharply, and the corrosion inhibition efficiency will decrease when the concentration reaches 200 mg/L. This phenomenon might be attributed to an enhanced aggregation effect of Na-CDs at higher concentrations, resulting in reduced film formation on the metal surface, resulting in an increase in the area of the metal exposed to the corrosive solution.

Table 1
The average value of weight loss, corrosion rate and corrosion inhibition efficiency of Q235 carbon steel soaked in 1 M HCl solution containing different concentrations of Na-CDs at 289 K for 24 h.

Content (mg/L)	ΔW(g)	V(g•cm^{-2}•h^{-1})	IE$_w$ (%)
0	0.8541 ± 0.0060	0.1627 ± 0.0007	
50	0.0795 ± 0.0067	0.0151 ± 0.0013	90.7039 ± 0.8384
100	0.0629 ± 0.0084	0.0119 ± 0.0016	92.6658 ± 0.9849
150	0.0384 ± 0.0070	0.0073 ± 0.0013	95.5180 ± 0.8217
200	0.0815 ± 0.0041	0.0156 ± 0.0008	90.4506 ± 0.4792

3.4. Electrochemical impedance spectroscopy analysis

Fig. 6(b-d) shows the Nyquist and Bode diagrams obtained by electrochemical impedance testing of Q235 carbon steel at 298 K temperature in 1 M HCl solution without or with different amounts of Na-CDs added. In the Nyquist plot (Fig. 6b), in the absence of Na-CDs, a large number of corrosion products are formed on the metal surface, and

Table 2
Potentiodynamic polarization data of Q235 carbon steel with different Na-CDs content in 1 M HCl.

$C_{Na\text{-}CDs}$ (mg/L)	E_{corr} (V)	I_{corr} (10^{-6} A/cm^2)	b_a (mV)	$-b_c$ (mV)	IE_{PDP} (%)
0	−0.42375	957.46	64.401	96.409	
50	−0.47823	99.607	75.009	51.052	89.60
100	−0.47344	71.264	60.703	44.764	92.56
150	−0.4807	45.782	49.353	40.576	95.22
200	−0.45953	116.52	83.002	72.448	87.83

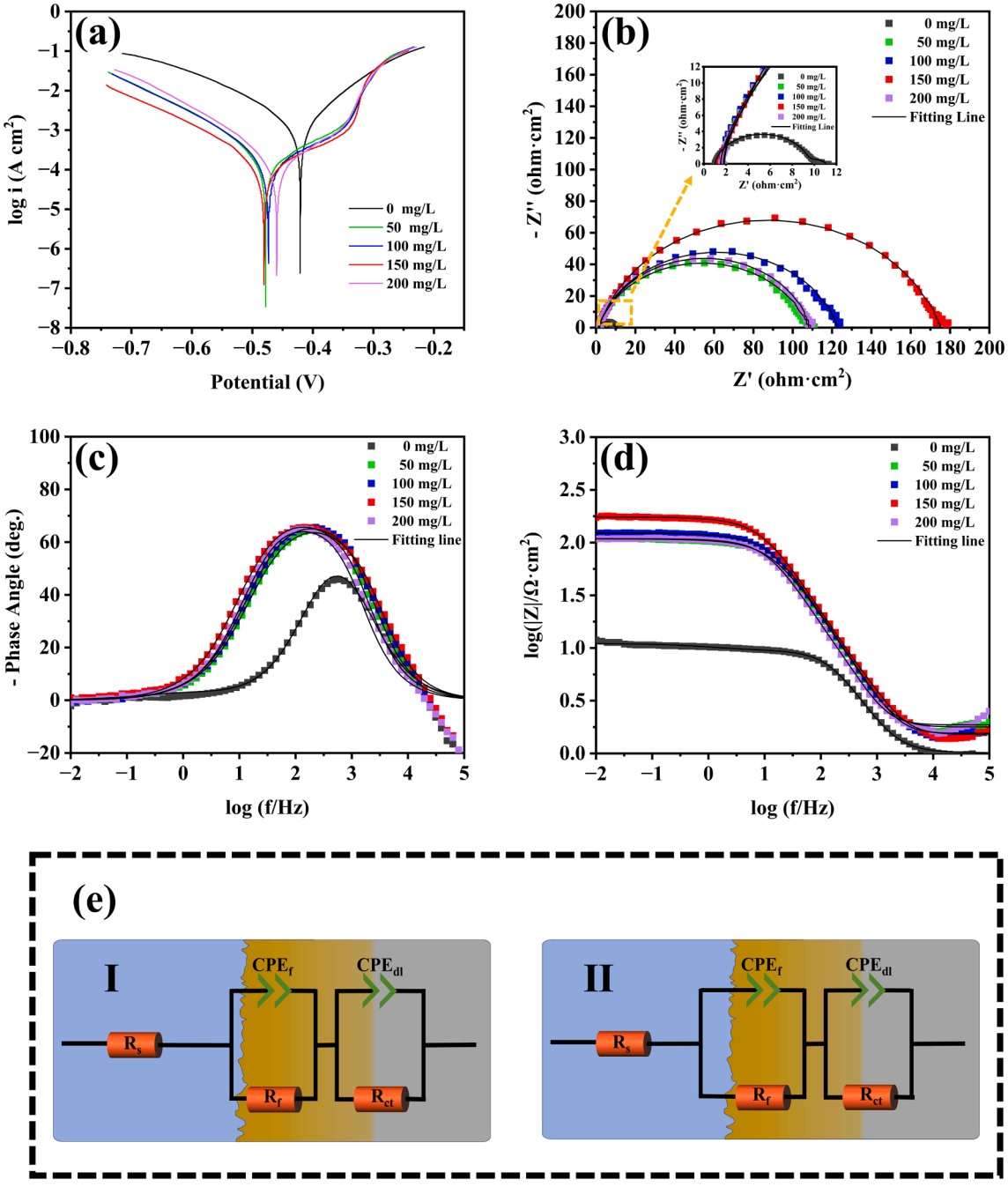

Fig. 6. PDP data result (a), EIS data result (b-d), and fitted circuit diagram (e).

a tailing phenomenon occurs in the capacitor loop. After the addition of Na-CDs, the radius of the capacitor ring significantly increased, indicating that the exposed active site area was reduced, and Na-CDs formed a protective layer on the metal surface, reducing the charge transfer rate, thereby inhibiting the corrosion of Q235 carbon steel in 1 M HCl solution (Luo et al., 2021b; Ouakki et al., 2020). The |Z| value at low frequencies also reflected the inhibitive performance of Na-CDs, with the |Z| value at 0.01 Hz increasing from 11.01 Ω·cm^2 in the blank to 175.09 Ω·cm^2 at a concentration of 150 mg/L, a 15.9-fold increase. As shown in Fig. 6c, the log10 (|Z|) increased from 1.04 to 2.25 Ω·cm^2. The phase angle data, as depicted in Fig. 6d, After the addition of Na-CDs, both show a wider Angle, which looks like the overlap of two angular peaks, indicating that the adsorption of Na-CDs on the Q235 carbon steel surface might be due to two reasons: 1) the double-layer capacitance (C_{dl}); and 2) the adsorption and desorption of Na-CDs at the metal/solution interface (Xu et al., 2023).

To better understand the EIS data, we used the equivalent circuit model as shown in Fig. 6f to fit the data, where I and II correspond to the fitted circuit after blank solution and Na-CDs addition, respectively. In the circuit, solution resistance, film resistance and charge transfer resistance are denoted by Rs, Rf and Rct respectively. At the same time, considering the non-homogeneity of the electrode, the ideal film capacitor (C_f) and double layer capacitor (C_{dl}) are replaced by CPE_f and CPE_{dl}. The impedance function of CPE can be calculated by equation (4) (Tan et al., 2020):

$$Z_{CPE} = Y_0^{-1}(j\omega)^{-n} \tag{4}$$

The impedance function of CPE was calculated using Equation (4), where Y_0 is the magnitude of the constant phase element, j is the imaginary unit, ω is the angular frequency, and n is the dispersion coefficient. When n equals −1, 0, or 1, the CPE represents an inductor, resistor, or capacitor, respectively. When n is between −1 and 1, it represents non-ideal capacitive or inductive behavior, and n can also be interpreted as an index of surface heterogeneity (Dong et al., 2023). The formulas for C_f and C_{dl} are shown in Equation (5).

$$C = Y_0(2\pi f_{z_{max}})^{n-1} \tag{5}$$

The inhibition efficiency IE_{EIS} of Na-CDs on Q235 carbon steel in 1 M HCl was calculated using Equations (6) and (7) (Y. Zhang et al., 2021). The resulting data, as shown in Table 3.

$$R_p = R_f + R_{ct} \tag{6}$$

$$IE_{EIS} = \frac{R_p - R_{p0}}{R_{p0}} \tag{7}$$

As indicated in Table 3, the EIS data were consistent with the weight loss tests and potentiodynamic polarization data, all of which demonstrated the highest efficiency at a concentration of 150 mg/L. In Table 3, the values of n_1 and n_2 were not integers in the absence of Na-CDs, suggesting that the electrochemical reactions on the metal surface under blank conditions were of a non-ideal dielectric nature. After the addition of the inhibitor, n_1 was consistently 1, while n_2 remained non-integer, indicating that the protective film formed by the inhibitor exhibited ideal capacitive behavior with the 1 M HCl solution, but the interface between the film and the metal was still characterized by non-ideal dielectric behavior. This could also be interpreted as the film formed by Na-CDs on the metal surface being heterogeneous. The resistances through the solution/film interface (R_f), the film/metal interface (R_{ct}), and their sum (R_p) revealed that both R_{ct} and R_p were at their maximum at a concentration of 150 mg/L. This could be understood to mean that at this concentration, the adsorption of Na-CDs on the metal surface was the most compact and the interaction with the metal was the strongest, resulting in the most dense and complete protective film. However, when the concentration exceeded this level, reaching 200 mg/L, the resistance provided by the film dropped sharply, indicating that the adsorption on the metal surface weakened and the film became less dense and complete, a conclusion consistent with that drawn from potentiodynamic polarization studies.

3.5. Adsorption isotherm and thermodynamic analyses

The adsorption process of inhibitors is of significant importance for studying the mechanism of corrosion inhibition. Different inhibitor systems are suitable for different adsorption isotherms. Goodness of fit R^2 can be used to judge whether the data fit the model adequately, and its value range is [0,1]. The closer the value is to 1, the better the fit. In the field of corrosion inhibitors, the most commonly used models are Langmuir and Freundlich isotherms. However, when the main body of the inhibitor is nanoparticles, these two adsorption isotherms are not suitable for direct application. This is because the aggregation effect and heterogeneity inherent to nanoparticles can have a certain impact on the adsorption process. Equations (8), (9), and (10) are the Langmuir, Freundlich, and Redlich-Peterson equations, respectively (Porkodi & Vasanth Kumar, 2007).

$$q_e = \frac{q_m K_{Langmuir} C_e}{1 + K_{Langmuir} C_e} \tag{8}$$

$$q_e = K_{Freundlich} C_e^{\frac{1}{n}} \tag{9}$$

$$q_e = \frac{AC_e}{1 + BC_e^{\alpha}} \tag{10}$$

q_e: Adsorption capacity

q_m: Maximum adsorption capacity, unit: mg/L.

$K_{Langmuir}$: Langmuir adsorption equilibrium constant, unit: L/mg.

C_e: Equilibrium concentration, unit: mg/L.

$K_{Freundlich}$: Adsorption equilibrium constant of Freundlich.

n: indicates the adsorption strength of the adsorbent.

A, B, α are parameters of the Redlich-Peterson model.

The Redlich-Peterson (R-P) adsorption isotherm is a three-parameter model that can, under certain conditions, be reduced to the Langmuir or Freundlich models (Wu et al., 2010). It incorporates characteristics of both the Langmuir and Freundlich models, allowing the R-P equation to describe the adsorption process on heterogeneous layers more accurately than the Langmuir and Freundlich isotherms (Wu et al., 2010). Considering the tendency of nanoparticles to aggregate and the microscopically uneven state of the metal surface, the R-P model was chosen to fit the data. According to Cen et al. (Cen et al., 2020) and Wu et al.

Table 3
Electrochemical impedance data of Q235 carbon steel with different Na-CDs content in 1 M HCl.

$C_{Na\text{-}CDs}$ (mg/L)	R_s (Ω cm^2)	CPE_f		C_f 10^{-5}F cm^2	R_f (Ω cm^2)	CPE_{dl}		C_{dl} 10^{-5}F cm^2	R_{ct} (Ω cm^2)	R_p (Ω cm^2)	IE_{EIS} (%)
		Y_{0f} (10^{-5} Ω^{-1} cm^{-2} s^n)	n_1			Y_{0dl} (10^{-5} Ω^{-1} cm^{-2} s^n)	n_2				
0	1.01	22.86	0.88	9.74	8.41	1901.00	0.64	270.20	1.64	10.05	
50	1.78	5.47	1.00	5.47	15.32	27.86	0.71	6.22	91.29	106.61	90.57
100	1.55	5.02	1.00	5.02	12.00	21.56	0.74	5.78	109.40	121.40	91.72
150	1.53	4.11	1.00	4.11	9.32	18.16	0.76	5.99	164.50	173.82	94.22
200	1.87	6.91	1.00	6.91	16.35	22.06	0.77	6.86	90.75	107.10	90.62

(Wu et al., 2010), the linear exponential expression has higher fitting accuracy than the linear logarithmic expression, converting Equation (10) to Equation (11).

$$C_e^{\alpha} = \frac{AC_e}{Bq_e} - \frac{1}{B} \tag{11}$$

In the adsorption process of nanoparticles as corrosion inhibitors, the value of α can represent the heterogeneity of the adsorption process. The closer the α value is to 1, the more it resembles monolayer adsorption. Ignoring the heterogeneity of the metal surface and considering it as an ideal solid surface, the effect of nanoparticle aggregation on the effective concentration for corrosion inhibition can be judged by the α value; the closer α is to 1, the less effect it has on the effective inhibition concentration (Cen et al., 2020; Dong et al., 2023).

The adsorption quantity q_e can typically be inferred by the surface coverage rate θ. The surface coverage rate θ is expressed as follows (Eq. (12)):

$$\theta = \frac{IE_{EIS}}{100} \tag{12}$$

The IE_{EIS} in Equation (10) can be obtained through Equation (5). By calculating and fitting the data using Excel and Origin, the α value (α = 1.15) was obtained. Substituting the α value into $(Ce)^{\alpha}$, the $(Ce)^{\alpha}$ value was obtained. A linear regression graph of Ce/qe versus $(Ce)^{\alpha}$ was plotted (Fig. 7a) with an R^2 value of 0.9987, slightly higher than that of the Langmuir fitting (Fig. 7b) with an R^2 of 0.9974. This result indicates that the R-P adsorption isotherm is more suitable than Langmuir isotherm to describe the adsorption process of carbon dot inhibitors on metal surface. As for the Freundlich isotherm, the results were clearly not applicable (Figure S1). Furthermore, according to the definition of the R-P equation and the fitting results, the adsorption of Na-CDs on the metal surface was very close to the ideal state described by the Langmuir adsorption. If the minimum heterogeneity of the metal surface and the weak interactions between the Na-CDs adsorbed on the metal surface, the adsorption–desorption equilibrium constant K_{ads} can be calculated to be 264.94 L/g according to Equation (8). The K_{ads} value depends on the adsorption capacity of the sample; the larger the K_{ads} value, the stronger the adsorption capacity. In addition, the standard Gibbs free energy ΔG^0_{ads} is an important physical quantity for studying the adsorption of inhibitors. When ΔG^0_{ads} is greater than -20 kJ/mol, it indicates a physisorption process, and when it is less than -40 kJ/mol, it indicates a chemisorption process. This can be calculated through Equation (13) (Zeng et al., 2022).

$$\Delta G^0_{ads} = -RTln(1000K_{ads}) \tag{13}$$

In this formula, R is 8.314 J/(mol·K), and T is the absolute temperature, which in this study is 289 K. By calculation, the value of ΔG^0_{ads} was found to be -30 kJ/mol. The value of Na-CDs is between -20 and -40 kJ/mol, which indicates that Na-CDs is adsorbed to the metal surface through a combined action of physical and chemical adsorption.

3.6. Corrosion morphology analyses

To better understand the corrosion inhibition mechanism of Na-CDs, SEM and EDS were used to analyze the corrosion morphology of Q235 carbon steel in its original state, as well as after soaking for 24 h in 1 M HCl solution without Na-CDs and with 150 mg/L Na-CDs (Fig. 8). It can be observed that the original metal surface (Fig. 8a) only exhibits scratches from polishing and is relatively smooth. In the 1 M HCl solution without Na-CDs, a large amount of corrosion products appeared (Fig. 8b), and the surface was significantly rougher than in its original state. After adding 150 mg/L Na-CDs, the corrosion products on the metal surface were greatly reduced, and the surface products appeared more like a thin film (Fig. 8c), which was obviously smoother than the metal surface soaked in the Na-CDs-free solution for 24 h. To further investigate the surface state of the metal and the film-forming nature of Na-CDs on the metal surface, EDS was performed on the region of Fig. 8 a1-c1 to analyze the elemental composition of the metal surface under different states.

The results obtained from EDS are shown in Fig. 9a-c, Figure S2, and Table S2. From Fig. 9a, it shows that the original Q235 steel mainly consists of Fe and C. After soaking for 24 h in 1 M HCl solution (Fig. 9b), the content of Fe atoms on the metal surface dropped sharply from 84.89 at% to 49.54 at%, the O content increased from 0.99 at% to 34.71 at%, and Cl atoms appeared on the surface (4.63 at%), indicating severe corrosion of the metal. In contrast to the metal in 1 M HCl solution, after adding Na-CDs (Fig. 9c), the Fe atom content on the metal surface increased, from 49.54 at% to 69.99 at%, while the O content decreased sharply (from 34.71 at% to 7.69 at%). This is because Na-CDs form a dense protective film on the Q235 carbon steel surface through both physical and chemical adsorption, inhibiting the dissolution of HCl on the steel (Zhu et al., 2021).

There are two noteworthy points. First, by comparing the metal surface states under different Na-CDs concentrations, it can be found that although the corrosion inhibition rates of different concentrations of Na-CDs is different, what is common is that they can all form good films on the metal surface (Figure S3), providing excellent protection to Q235 carbon steel, which corresponds to the results from the earlier weight loss tests and electrochemical tests. Another point to note is that by comparing the state of the metal at a concentration of 150 mg/L with and without slow rinsing with deionized water (Figure S4), it can be found that the morphology of the products on the metal surface is different, but after slow rinsing with deionized water, there will no longer be large particle agglomerations on the metal surface, and the

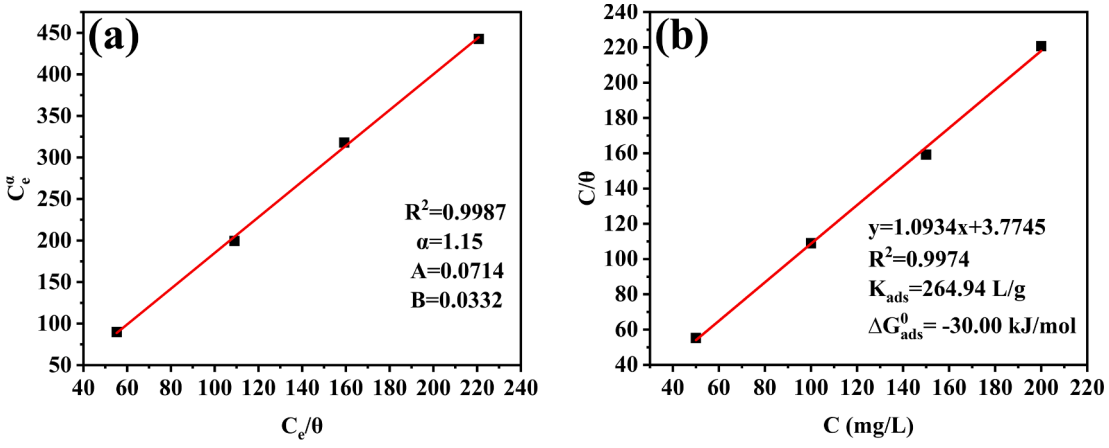

Fig. 7. Isotherm adsorption curves of (a) R-P, (b) Langmuir.

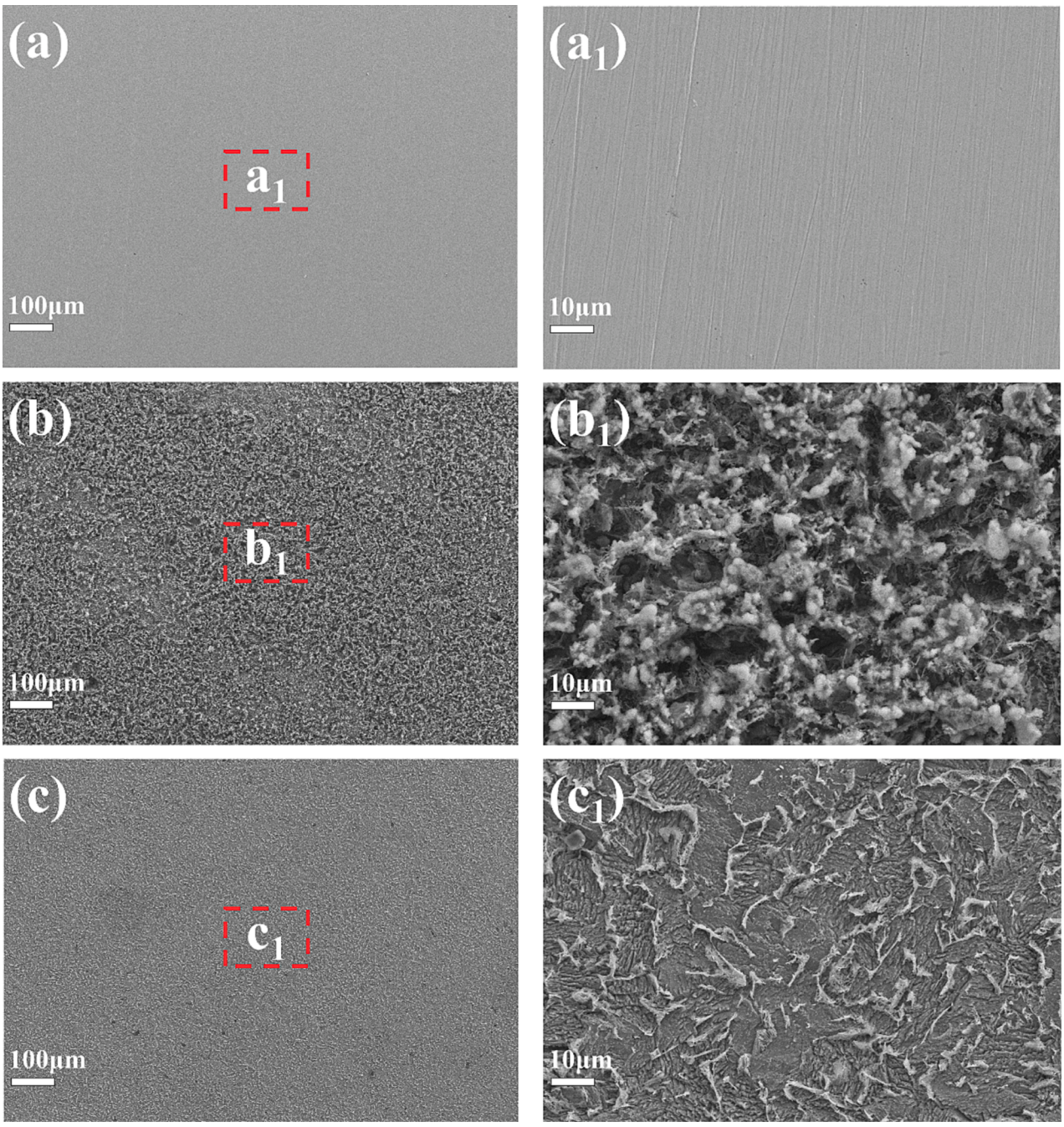

Fig. 8. Q235 carbon steel morphologies in different states.

contents of Cl and O decrease sharply. This indicates that Na from Na-CDs combines with Cl ions to form NaCl on the metal surface, which is rapidly lost with the rinsing water, consistent with the earlier speculation.

3.7. Inhibition mechanism for Na-CDs

As shown by FRIT and XPS, Na-CDs are composed of Na, C, O, and are rich in hydroxyl, carboxyl, and carbonyl groups. The good agreement between the weight loss tests and electrochemical test results suggests that Na-CDs are most effective at 150 mg/L in 1 M HCl solution for Q235 carbon steel. The Zeta potential results show that Na-CDs become positively charged (24.8 mV) in 1 M HCl solution, while the iron surface is negatively charged in hydrochloric acid. Therefore, Na-CDs will adsorb onto the metal surface through electrostatic attraction. Additionally, through adsorption analysis and analysis of different states of the metal surface, it is known that the film formation of Na-CDs on the metal surface is formed by the combined action of physical and chemical adsorption, which is consistent with the electrochemical test results. At 150 mg/L, Na-CDs have the strongest adsorption capacity on the metal surface, and the film formed is the most complete and dense. However, when the concentration exceeds 150 mg/L, the interaction between nanoparticles increases, leading to desorption of Na-CDs from the metal surface, thereby reducing the density and integrity of the protective film. To more intuitively explain this phenomenon, this study proposes the corrosion inhibitor mechanism shown in Fig. 10. As illustrated in Fig. 8, when Na-CDs are added to the solution, they first adsorb onto the metal surface to form a film, with Cl ions playing a bridging role. When the concentration of the inhibitor is further increased, the interaction between Na-CDs strengthens, leading to desorption from the metal surface

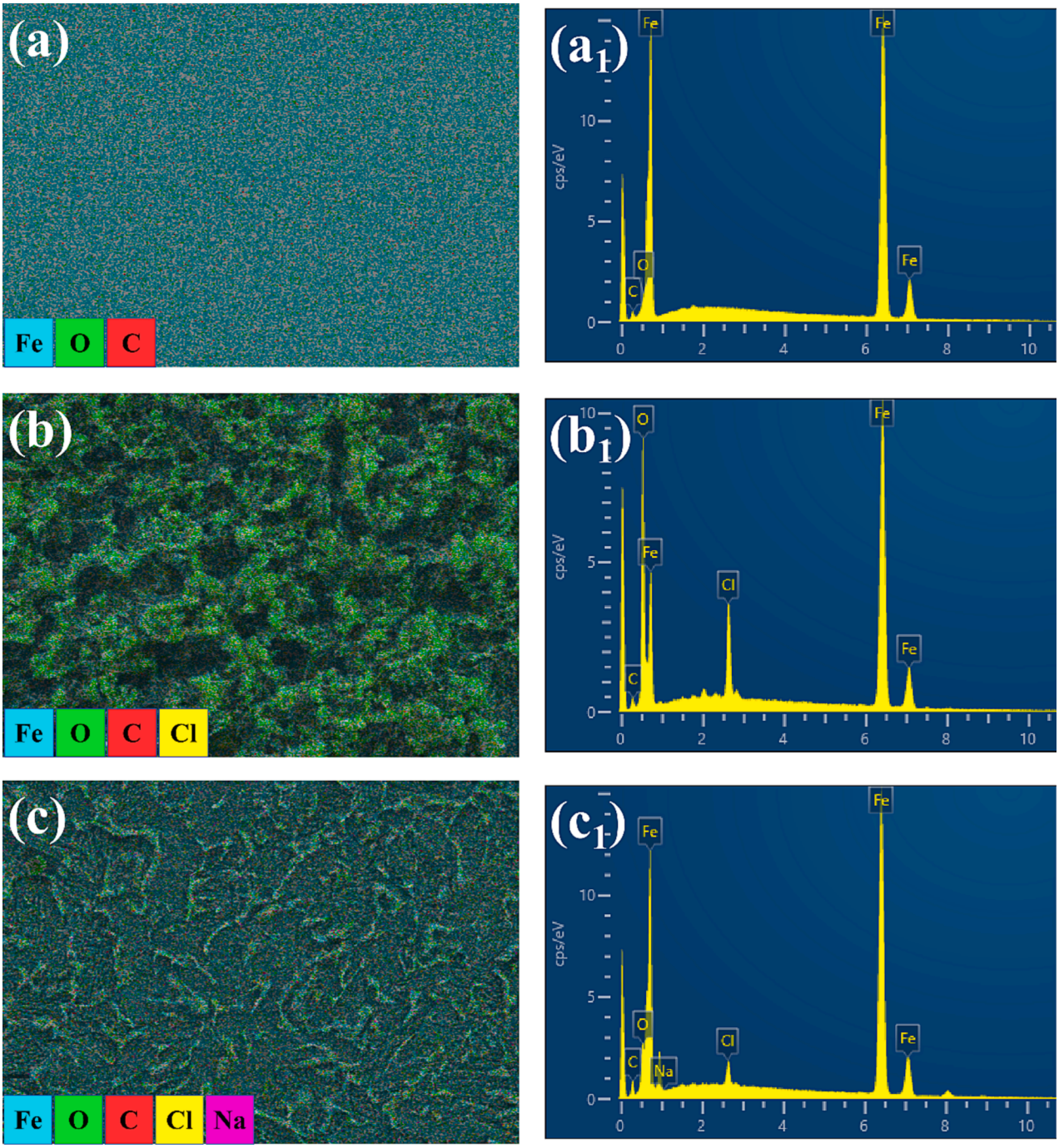

Fig. 9. EDS data of Q235 carbon steel in different states.

and reducing the density and integrity of the film.

4. Conclusions

Green and highly efficient Na-CDs corrosion inhibitors have been synthesized via a hydrothermal method. Detailed characterization analysis and investigation into their corrosion inhibition behavior for Q235 steel in 1 M HCl have led to the following conclusions:

(1) The Na-CDs exhibit an average particle size of 3.62 nm with a relatively uniform distribution, primarily ranging between 2 and 5 nm.

(2) The Na-CDs have proven to be effective in protecting Q235 steel in 1 M HCl, achieving a corrosion inhibition efficiency of up to 96 % at a concentration of 150 mg/L. The inhibition efficiency increases with concentration initially but decreases after reaching a certain level.

(3) The adsorption of Na-CDs on the metal surface follows the R-P adsorption isotherm, approaching the ideal state of monolayer homogeneous adsorption.

(4) The protection of the metal by Na-CDs primarily stems from their ability to form a protective layer on the metal surface through both physical and chemical adsorption, with Cl ions in the HCl solution playing a bridging role.

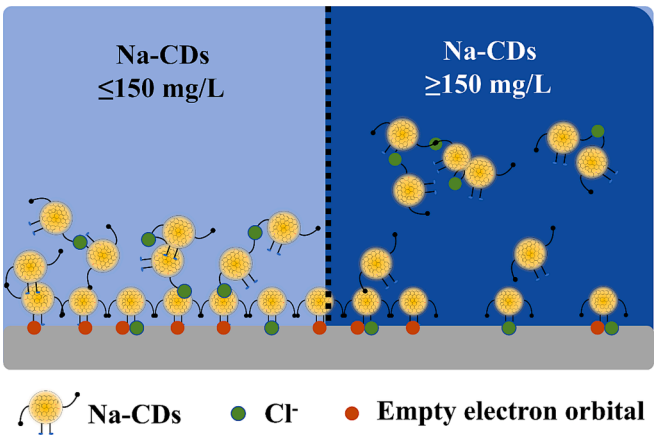

Fig. 10. Corrosion inhibition mechanism diagram.

CRediT authorship contribution statement

Liming Dong: Conceptualization, Validation, Writing – original draft, Writing – review & editing. **Jingbao Wang:** Data curation, Validation, Investigation, Project administration. **Yuyue Ma:** Data curation. **Yilei Ruan:** Investigation. **Zhiyong Hu:** Supervision. **Xuemei Ma:** Conceptualization, Methodology, Writing – original draft, Writing – review & editing.

Declaration of competing interest

The authors declare that they have no known competing financial interests or personal relationships that could have appeared to influence the work reported in this paper.

Acknowledgments

This work was supported by the Shanxi Key Laboratory of Advanced Carbon Electrode Materials (No. 202104010910019) and the Shanxi Scholarship Council of China (No. 2022–137).

Appendix A. Supplementary material

Supplementary data to this article can be found online at https://doi.org/10.1016/j.arabjc.2024.105660.

References

Abd El-Lateef, H.M., Abo-Riya, M.A., Tantawy, A.H., 2016. Empirical and quantum chemical studies on the corrosion inhibition performance of some novel synthesized cationic gemini surfactants on carbon steel pipelines in acid pickling processes. Corros. Sci. 108, 94–110. https://doi.org/10.1016/j.corsci.2016.03.004.

Abdelhameed, M., Jevasuwan, W., Subramani, T., Chen, J., Fukata, N., 2021. Efficiency enhancement of Si nanostructure hybrid solar cells by optimizing non-radiative energy transfer from Si quantum dots. Nano Energy 82, 105728. https://doi.org/10.1016/j.nanoen.2020.105728.

Ai, L., Pei, Y., Song, Z., Yong, X., Song, H., Liu, G., Nie, M., Waterhouse, G.I.N., Yan, X., Lu, S., 2023. Ligand-Triggered Self-Assembly of Flexible Carbon Dot Nanoribbons for Optoelectronic Memristor Devices and Neuromorphic Computing. Adv. Sci. https://doi.org/10.1002/advs.202207688.

Almomani, M.S., Ahmed, N.M., Rashid, M., Almessiere, M.A., Altowyan, A.S., 2021. White, blue and green emission from Si QDs derived from zinc incorporated porous silicon. J. Lumin. 232, 117845 https://doi.org/10.1016/j.jlumin.2020.117845.

Cao, C., Guo, W., 2024. Carbon dots-based fluorescent probe for the detection of imidacloprid residue in leafy vegetables. Food Chem. 435, 137578 https://doi.org/10.1016/j.foodchem.2023.137578.

Cen, H., Chen, Z., Guo, X., 2019a. N, S co-doped carbon dots as effective corrosion inhibitor for carbon steel in CO2-saturated 3.5% NaCl solution. J. Taiwan Inst. Chem. Eng. 99, 224–238. https://doi.org/10.1016/j.jtice.2019.02.036.

Cen, H., Zhang, X., Zhao, L., Chen, Z., Guo, X., 2019b. Carbon dots as effective corrosion inhibitor for 5052 aluminium alloy in 0.1 M HCl solution. Corros. Sci. 161, 108197 https://doi.org/10.1016/j.corsci.2019.108197.

Cen, H., Cao, J., Chen, Z., 2020. Functionalized carbon nanotubes as a novel inhibitor to enhance the anticorrosion performance of carbon steel in CO2-saturated NaCl solution. Corros. Sci. 177, 109011 https://doi.org/10.1016/j.corsci.2020.109011.

Cui, R., Gu, N., Li, C., 2011. Polyaspartic acid as a green corrosion inhibitor for carbon steel. Mater. Corros. 62 (4), 362–369. https://doi.org/10.1002/maco.200905511.

Cui, M., Ren, S., Xue, Q., Zhao, H., Wang, L., 2017. Carbon dots as new eco-friendly and effective corrosion inhibitor. J. Alloy. Compd. 726, 680–692. https://doi.org/10.1016/j.jallcom.2017.08.027.

Dang, D.K., Sundaram, C., Ngo, Y.-L.-T., Chung, J.S., Kim, E.J., Hur, S.H., 2018. One pot solid-state synthesis of highly fluorescent N and S co-doped carbon dots and its use as fluorescent probe for Ag+ detection in aqueous solution. Sens. Actuators B 255, 3284–3291. https://doi.org/10.1016/j.snb.2017.09.155.

Desimone, M.P., Grundmeier, G., Gordillo, G., Simison, S.N., 2011. Amphiphilic amido-amine as an effective corrosion inhibitor for mild steel exposed to CO2 saturated solution: Polarization. EIS and PM-IRRAS Studies. *Electrochimica Acta* 56 (8), 2990–2998. https://doi.org/10.1016/j.electacta.2011.01.009.

Dong, L., Ma, Y., Jin, X., Feng, L., Zhu, H., Hu, Z., Ma, X., 2023. High-Efficiency Corrosion Inhibitor of Biomass-Derived High-Yield Carbon Quantum Dots for Q235 Carbon Steel in 1 M HCl Solution. ACS Omega. https://doi.org/10.1021/acsomega.3c06702.

El-Etre, A.Y., Abdallah, M., El-Tantawy, Z.E., 2005. Corrosion inhibition of some metals using lawsonia extract. Corros. Sci. 47 (2), 385–395. https://doi.org/10.1016/j.corsci.2004.06.006.

García de Arquer, F.P., Talapin, D.V., Klimov, V.I., Arakawa, Y., Bayer, M., Sargent, E.H., 2021. Semiconductor quantum dots: Technological progress and future challenges. Science 373 (6555), eaaz8541. https://doi.org/10.1126/science.aaz8541.

Guo, Y., Lay, C.-H., Zhou, D., Dong, S., Zhang, J., Ren, N., 2020. Enhanced photocatalytic performance of metal silver and carbon dots co-doped BiOI photocatalysts and mechanism investigation. Environ. Sci. Pollut. Res. 27 (15), 17516–17529. https://doi.org/10.1007/s11356-019-05684-z.

Gutiérrez, E., Rodríguez, J.A., Cruz-Borbolla, J., Alvarado-Rodríguez, J.G., Thangarasu, P., 2016. Development of a predictive model for corrosion inhibition of carbon steel by imidazole and benzimidazole derivatives. Corros. Sci. 108, 23–35. https://doi.org/10.1016/j.corsci.2016.02.036.

Han, B., Peng, T., Yu, M., Chi, C., Li, Y., Hu, X., He, G., 2018. One-pot synthesis of highly fluorescent Fe2+-doped carbon dots for a dual-emissive nanohybrid for the detection of zinc ions and histidine. New J. Chem. 42 (16), 13651–13659. https://doi.org/10.1039/C8NJ01858H.

Hejazi, S., Mohajernia, S.h., Moayed, M.H., Davoodi, A., Rahimizadeh, M., Momeni, M., Eslami, A., Shiri, A., Kosari, A., 2015. Electrochemical and quantum chemical study of Thiazolo-pyrimidine derivatives as corrosion inhibitors on mild steel in 1M H2SO4. J. Ind. Eng. Chem. 25, 112–121. https://doi.org/10.1016/j.jiec.2014.10.020.

Hu, Z., Meng, Y., Ma, X., Zhu, H., Li, J., Li, C., Cao, D., 2016. Experimental and theoretical studies of benzothiazole derivatives as corrosion inhibitors for carbon steel in 1 M HCl. Corros. Sci. 112, 563–575. https://doi.org/10.1016/j.corsci.2016.08.012.

Jin, X., Wang, J., Zheng, S., Li, J., Ma, X., Feng, L., Zhu, H., Hu, Z., 2022. The study of surface activity and anti-corrosion of novel surfactants for carbon steel in 1 M HCl. J. Mol. Liq. 353, 118747 https://doi.org/10.1016/j.molliq.2022.118747.

Li, X., Fu, Y., Zhao, S., Xiao, J., Lan, M., Wang, B., Zhang, K., Song, X., Zeng, L., 2022. Metal ions-doped carbon dots: Synthesis, properties, and applications. Chem. Eng. J. 430, 133101 https://doi.org/10.1016/j.cej.2021.133101.

Li, W., Liu, Y., Wang, B., Song, H., Liu, Z., Lu, S., Yang, B., 2019. Kilogram-scale synthesis of carbon quantum dots for hydrogen evolution, sensing and bioimaging. Chin. Chem. Lett. 30 (12), 2323–2327. https://doi.org/10.1016/j.cclet.2019.06.040.

Liu, X., Wang, J., Wu, D., Wang, Z., Li, Y., Fan, X., Zhang, F., Zhang, G., Peng, W., 2022. N-doped carbon dots decorated 3D g-C3N4 for visible-light driven peroxydisulfate activation: Insights of non-radical route induced by Na+ doping. Appl Catal B 310, 121304. https://doi.org/10.1016/j.apcatb.2022.121304.

Liu, Z., Ye, Y.W., Chen, H., 2020. Corrosion inhibition behavior and mechanism of N-doped carbon dots for metal in acid environment. J. Clean. Prod. 270, 122458 https://doi.org/10.1016/j.jclepro.2020.122458.

Luo, J., Cheng, X., Chen, X., Zhong, C.F., Xie, H., Ye, Y.W., Zhao, H.C., Li, Y., Chen, H., 2021a. The effect of N and S ratios in N, S co-doped carbon dot inhibitor on metal protection in 1 M HCl solution. J. Taiwan Inst. Chem. Eng. 127, 387–398. https://doi.org/10.1016/j.jtice.2021.08.023.

Luo, J., Cheng, X., Zhong, C., Chen, X., Ye, Y.W., Zhao, H., Chen, H., 2021b. Effect of reaction parameters on the corrosion inhibition behavior of N-doped carbon dots for metal in 1 M HCl solution. J. Mol. Liq. 338, 116783 https://doi.org/10.1016/j.molliq.2021.116783.

Miao, X., Qu, D., Yang, D., Nie, B., Zhao, Y., Fan, H., Sun, Z., 2018. Synthesis of Carbon Dots with Multiple Color Emission by Controlled Graphitization and Surface Functionalization. Adv. Mater. 30 (1), 1704740. https://doi.org/10.1002/adma.201704740.

Mu, Z., Hua, J., Kumar Tammina, S., Yang, Y., 2019. Visible light photocatalytic activity of Cu, N co-doped carbon dots/Ag3PO4 nanocomposites for neutral red under green LED radiation. Colloids Surf A Physicochem Eng Asp 578, 123643. https://doi.org/10.1016/j.colsurfa.2019.123643.

Ouakki, M., Galai, M., Rbaa, M., Abousalem, A.S., Lakhrissi, B., Rifi, E.H., Cherkaoui, M., 2020. Investigation of imidazole derivatives as corrosion inhibitors for mild steel in sulfuric acidic environment: Experimental and theoretical studies. Ionics 26 (10), 5251–5272. https://doi.org/10.1007/s11581-020-03643-0.

Padhan, S., Rout, T.K., Nair, U.G., 2022. N-doped and Cu, N-doped carbon dots as corrosion inhibitor for mild steel corrosion in acid medium. Colloids Surf A

Physicochem Eng Asp 653, 129905. https://doi.org/10.1016/j.colsurfa.2022.129905.
Porkodi, K., Vasanth Kumar, K., 2007. Equilibrium, kinetics and mechanism modeling and simulation of basic and acid dyes sorption onto jute fiber carbon: Eosin yellow, malachite green and crystal violet single component systems. J. Hazard. Mater. 143 (1), 311–327. https://doi.org/10.1016/j.jhazmat.2006.09.029.
Qiang, Y., Zhang, S., Guo, L., Zheng, X., Xiang, B., Chen, S., 2017. Experimental and theoretical studies of four allyl imidazolium-based ionic liquids as green inhibitors for copper corrosion in sulfuric acid. Corros. Sci. 119, 68–78. https://doi.org/10.1016/j.corsci.2017.02.021.
Ramezanzadeh, M., Bahlakeh, G., Sanaei, Z., Ramezanzadeh, B., 2019. Corrosion inhibition of mild steel in 1 M HCl solution by ethanolic extract of eco-friendly Mangifera indica (mango) leaves: Electrochemical, molecular dynamics, Monte Carlo and ab initio study. Appl. Surf. Sci. 463, 1058–1077. https://doi.org/10.1016/j.apsusc.2018.09.029.
Rashid, I., Omari, M.H.A., Leharne, S.A., Chowdhry, B.Z., Badwan, A., 2012. Starch gelatinization using sodium silicate: FTIR, DSC, XRPD, and NMR studies. Starch - Stärke 64 (9), 713–728. https://doi.org/10.1002/star.201100190.
Ren, S., Cui, M., Chen, X., Mei, S., Qiang, Y., 2022. Comparative study on corrosion inhibition of N doped and N, S codoped carbon dots for carbon steel in strong acidic solution. J. Colloid Interface Sci. 628, 384–397. https://doi.org/10.1016/j.jcis.2022.08.070.
Ren, X., Liu, J., Ren, J., Tang, F., Meng, X., 2015. One-pot synthesis of active copper-containing carbon dots with laccase-like activities. Nanoscale 7 (46), 19641–19646. https://doi.org/10.1039/C5NR04685H.
Saraswat, V., Yadav, M., 2021. Improved corrosion resistant performance of mild steel under acid environment by novel carbon dots as green corrosion inhibitor. Colloids Surf A Physicochem Eng Asp 627, 127172. https://doi.org/10.1016/j.colsurfa.2021.127172.
Tan, J., Guo, L., Yang, H., Zhang, F., El Bakri, Y., 2020. Synergistic effect of potassium iodide and sodium dodecyl sulfonate on the corrosion inhibition of carbon steel in HCl medium: A combined experimental and theoretical investigation. RSC Adv. 10 (26), 15163–15170. https://doi.org/10.1039/D0RA02011G.
Tian, J., Chen, J., Liu, J., Tian, Q., Chen, P., 2018. Graphene quantum dot engineered nickel-cobalt phosphide as highly efficient bifunctional catalyst for overall water splitting. Nano Energy 48, 284–291. https://doi.org/10.1016/j.nanoen.2018.03.063.
Wang, J., Jing, J., Feng, L., Zhu, H., Hu, Z., Ma, X., 2021. Study on corrosion inhibition behavior and adsorption mechanism of novel synthetic surfactants for carbon steel in 1 M HCl solution. Sustain. Chem. Pharm. 23, 100500 https://doi.org/10.1016/j.scp.2021.100500.
Wang, L., Wang, Y., Xu, T., Liao, H., Yao, C., Liu, Y., Li, Z., Chen, Z., Pan, D., Sun, L., Wu, M., 2014. Gram-scale synthesis of single-crystalline graphene quantum dots with superior optical properties. *Nature*. Communications 5(1), Article 1. https://doi.org/10.1038/ncomms6357.
Wu, F.-C., Liu, B.-L., Wu, K.-T., Tseng, R.-L., 2010. A new linear form analysis of Redlich-Peterson isotherm equation for the adsorptions of dyes. Chem. Eng. J. 162 (1), 21–27. https://doi.org/10.1016/j.cej.2010.03.006.
Xu, Z., Gan, Y., Zeng, J., Chen, J., Fu, A., Zheng, X., Li, W., 2023. Green synthesis of functionalized fluorescent carbon dots from biomass and their corrosion inhibition mechanism for copper in sulfuric acid environment. Chem. Eng. J. 470, 144425 https://doi.org/10.1016/j.cej.2023.144425.
Yang, Q., Duan, J., Yang, W., Li, X., Mo, J., Yang, P., Tang, Q., 2018. Nitrogen-doped carbon quantum dots from biomass via simple one-pot method and exploration of their application. Appl. Surf. Sci. 434, 1079–1085. https://doi.org/10.1016/j.apsusc.2017.11.040.
Yang, D., Ye, Y., Su, Y., Liu, S., Gong, D., Zhao, H., 2019. Functionalization of citric acid-based carbon dots by imidazole toward novel green corrosion inhibitor for carbon steel. J. Clean. Prod. 229, 180–192. https://doi.org/10.1016/j.jclepro.2019.05.030.
Ye, Y., Yang, D., Chen, H., Guo, S., Yang, Q., Chen, L., Zhao, H., Wang, L., 2020. A high-efficiency corrosion inhibitor of N-doped citric acid-based carbon dots for mild steel in hydrochloric acid environment. J. Hazard. Mater. 381, 121019 https://doi.org/10.1016/j.jhazmat.2019.121019.
Zeng, S., Zhang, F., Liu, Y., Ouyang, S., Ye, Y.W., Chen, H., 2022. Synthesis of Ce, N co–doped carbon dots as green and effective corrosion inhibitor for copper in acid environment. J. Taiwan Inst. Chem. Eng. 141, 104608 https://doi.org/10.1016/j.jtice.2022.104608.
Zhang, K., 2018. Amino acids modified konjac glucomannan as green corrosion inhibitors for mild steel in HCl solution. Carbohydr. Polym. 9.
Zhang, Y., Nie, M., Wang, X., Zhu, Y., Shi, F., Yu, J., Hou, B., 2015. Effect of molecular structure of aniline–formaldehyde copolymers on corrosion inhibition of mild steel in hydrochloric acid solution. J. Hazard. Mater. 289, 130–139. https://doi.org/10.1016/j.jhazmat.2015.02.036.
Zhang, X., Wang, F., He, Y., Du, Y., 2001. Study of the inhibition mechanism of imidazoline amide on CO2 corrosion of Armco iron. Corros. Sci. 43 (8), 1417–1431. https://doi.org/10.1016/S0010-938X(00)00160-8.
Zhang, Y., Zhang, S., Tan, B., Guo, L., Li, H., 2021. Solvothermal synthesis of functionalized carbon dots from amino acid as an eco-friendly corrosion inhibitor for copper in sulfuric acid solution. J. Colloid Interface Sci. 604, 1–14. https://doi.org/10.1016/j.jcis.2021.07.034.
Zhao, H., Sun, T.-Y., Huang, L.-F., Wei, J., Qiu, S., 2022. A green strategy for nitrogen-doped polymer nanodots with high oxygen and chloride corrosion resistance in extremely acidic condition. Chem. Eng. J. 437, 135242 https://doi.org/10.1016/j.cej.2022.135242.
Zhu, M., He, Z., Guo, L., Zhang, R., Anadebe, V.C., Obot, I.B., Zheng, X., 2021. Corrosion inhibition of eco-friendly nitrogen-doped carbon dots for carbon steel in acidic media: Performance and mechanism investigation. J. Mol. Liq. 342, 117583 https://doi.org/10.1016/j.molliq.2021.117583.
Zhu, M., Guo, L., He, Z., Marzouki, R., Zhang, R., Berdimurodov, E., 2022. Insights into the newly synthesized N-doped carbon dots for Q235 steel corrosion retardation in acidizing media: A detailed multidimensional study. J. Colloid Interface Sci. 608, 2039–2049. https://doi.org/10.1016/j.jcis.2021.10.160.